

Ab Initio Modeling of the Interaction of Electron Beams and Single-Walled Carbon NanotubesA. Nojeh,^{1,*} B. Shan,² K. Cho,³ and R. F. W. Pease¹¹Department of Electrical Engineering, Stanford University, Stanford, California 94305, USA²Department of Applied Physics, Stanford University, Stanford, California 94305, USA³Department of Mechanical Engineering, Stanford University, Stanford, California 94305, USA

(Received 23 August 2005; published 9 February 2006)

Single-walled carbon nanotubes are readily observable in a scanning electron microscope, which traditional models fail to explain. We present an *ab initio* model to explain how the electron beam can interact with these structures despite the very small, nanoscale, interaction volume. In particular, we show how the electron beam can generate very strong secondary electron emission from the tip of a nanotube under external electric field. The approach may also be used in modeling the interaction of charged particles with nanostructures in other applications such as electron detection.

DOI: 10.1103/PhysRevLett.96.056802

PACS numbers: 73.22.-f, 79.70.+q, 79.90.+b

Introduction.—The strong mechanical structure, ability to carry extremely high current densities (10^9 A/cm²), and high aspect ratio make single-walled carbon nanotubes (SWNTs) very promising candidates for application as electron emitters [1–3]. Controlled emission from a SWNT tip means a nanometer-size emission spot, which could lead to the formation of a very sharp electron beam. At the same time, despite extremely small diameters, SWNTs are readily observable in a scanning electron microscope (SEM). In particular, if a SWNT is biased near the field-emission threshold while being looked at inside an SEM, every time the primary beam of the SEM hits the nanotube tip during a scan, a large number of secondary electrons are emitted from the tip [4,5]. This emission stops once the primary beam has gone past the nanotube tip. This large secondary emission only during the short time when the primary beam is on the nanotube tip appears as a distinct bright spot on the image (Fig. 1). Because of the small dimensions in question, such high secondary electron emission from the nanotube and, in particular, its tip cannot be explained by traditional beam-specimen models that treat the sample as a bulk where the electron beam undergoes multiple scatterings and gradually loses energy to the sample. On the other hand, since imaging nanodevices is of crucial importance to research in nanotechnology and the (SEM) remains one of the main workhorses of the imaging world, it is necessary to develop a proper model that can account for the interaction of the SEM electron beam and nanotubes. Electron emission from SWNTs caused by external electric field has previously been studied [6–9]. Here, we present an *ab initio* model to explain electron emission from SWNTs induced by another electron beam, such as in the SEM.

The model.—When electrons in the primary beam of an SEM hit a bulk material, they undergo a large number of scatterings. This gives them a good chance of generating secondary electrons. These scattering phenomena have been studied extensively, and the process of secondary electron generation is usually modeled using Monte Carlo methods [10]. These models are well capable of explaining

the behavior of bulk materials in the SEM. However, a SWNT has a diameter on the order of a nanometer, and is hollow. It is hard to imagine that an incoming electron with the energy of several keV sees the nanotube as a big obstacle and is strongly scattered by its lattice. Therefore, the traditional models may not be well suited to explain the type of interaction between the primary electrons and the electrons inside the nanotube. Here, we suggest the following model.

When an electron from the SEM primary beam (several keV kinetic energy) hits the nanotube surface, it might induce a weak secondary emission from the monolayer graphitic shell, but this would not lead to the highly bright nanotube image, especially since graphite has poor secondary emission yield. This weak interaction with the nanotube surface does not slow down the high-energy primary electron significantly, and thus the electron penetrates the nanotube. Once inside the nanotube, its associated electrostatic potential raises the nanotube energy levels significantly, and makes it easy for the nanotube electrons to overcome the work function barrier, thus leading to strong secondary emission. In particular, if a nanotube is biased at a negative voltage near the field-emission

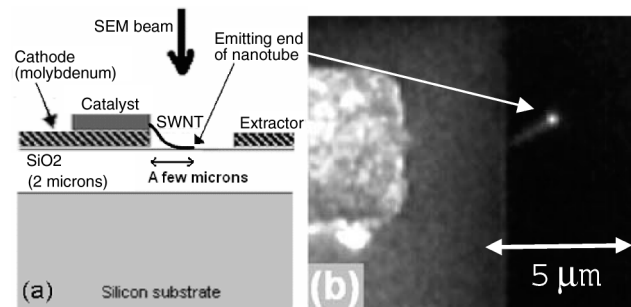


FIG. 1. (a) Schematic of the device cross section. (b) Cathode (left electrode) held at -140 V. Extractor (right electrode—not visible) held at ground. Note that the negative electrode is bright due to voltage contrast. Stimulated electron emission from the tip of the nanotube has started.

threshold, a large number of electrons from the negative power supply are drawn to the nanotube tip where the electric field is the strongest (field enhancement because of sharp geometry can be as much as 1000 times [11,12]). These electrons are on the threshold of emission and only a small extra “kick” from the primary beam can send them out to vacuum, leading to very bright spots on the image.

We used *ab initio* simulations to obtain the energy levels and investigate their behavior as a result of the presence of the primary beam electrons. Because of the extremely time-expensive nature of these calculations, we used a small system: 4 unit cells of a (5, 5) nanotube (diameter ~ 6.8 Å). Other authors have used short nanotubes to simulate normal field emission [8,11,12]. To compensate for the short length, they used an external field value that already contains the effect of field enhancement because of sharp nanotube geometry. This is further validated by the calculations presented in [13], where the authors employed a hybrid quantum mechanics–molecular mechanics approach that enabled them to examine field enhancement by a micron long nanotube. The nanotube coordinates were generated using the FORTRAN programs presented in [14]. One side was capped with one-half of a C_{60} molecule, and the other side was terminated with hydrogen atoms to eliminate the dangling bonds. We relaxed the structure using molecular dynamics with Brenner-Tersoff-type potentials. Then we used the program GAUSSIAN [15] to perform the energy calculations, with a Hartree-Fock (HF) model and a 6-31G(d) basis set. The final nonuniform electric field distribution in space is calculated by taking into account the externally applied field, as well as the field due to the rearrangement of charge in the nanotube in response to the external field, in a self-consistent scheme. Although the HF level of theory does not include electron correlations and is not accurate in reproducing the unoccupied orbitals, it provides a good description of the valence band [16] and has been shown to reproduce the ionization energies of several molecular systems within 1 eV (usually an overestimate) [17], which is relevant to the present study. Also, HF calculations are much faster than density functional theory (DFT) calculations, which tend to slightly underestimate the ionization energies. Finally, in order to fully justify our use of the HF model, we repeated some of the calculations with DFT for comparison.

Results and discussion.—First, we calculated the energy levels of the nanotube without any applied electric field or primary beam electrons [Fig. 2(a)]. The occupied orbitals were all below the vacuum level as expected, with the highest occupied molecular orbital (HOMO) at -5.11 eV. This is in good agreement with nanotube work functions known to be around 5 eV and is a further justification of our use of the HF level of theory. For comparison, we repeated the calculation with DFT (model B3LYP) and obtained -4.5 eV for HOMO. Also, the HOMO and a few orbitals below it were widely distributed in space [not localized to the tip region—Fig. 2(b)]. Then, we applied an external

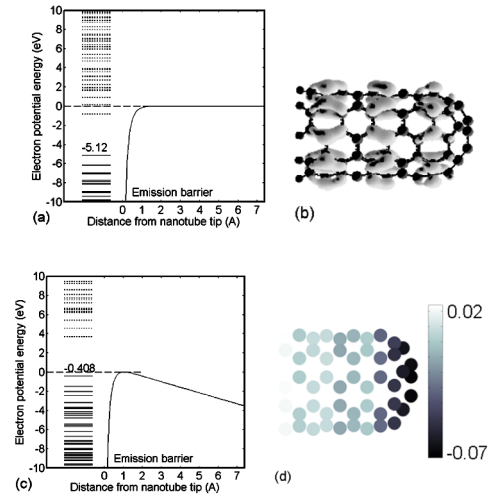


FIG. 2 (color online). (a) Energy levels around the Fermi level and potential barrier at the tip of the nanotube with no external field (HOMO = -5.11 eV). Solid lines represent occupied orbitals, and dashed lines represent unoccupied orbitals. (b) Spatial distribution of HOMO at no external field. (c) Energy levels in the presence of an extraction field of ~ 0.5 V/Å along the nanotube axis. (d) Difference in charge distribution between cases with and without a ~ 1 V/Å external field. Darker regions correspond to a higher concentration of negative charge. Note the localization at the tip due to the field.

electric field of ~ 0.5 V/Å (typical of the field at the tube tip in electron emission experiments, including the field-enhancement effect) along the nanotube axis. We plotted the potential barrier along the nanotube axis by summing the electronic potential energy due to the nanotube (including the effect of the charge redistribution in it) and that due to the external field [Fig. 2(c)]. As we see, the external field induced a slope in the vacuum level outside the tube, as well as an upward shift in the molecular energy levels. This makes them more susceptible to tunneling out of the material and emission, because each level now sees a narrower tunneling barrier than before. When the field intensity was raised even more (to ~ 1 V/Å), some of the occupied orbitals rose above the emission barrier (HOMO was 3.24 eV above the barrier top), which suggests very strong emission from the nanotube. Also, negative charge was attracted toward the tip because of the field. In order to visualize the effect of the field in displacing all the orbitals, we plotted the difference in electronic charge distribution (which is the sum of contributions from all orbitals) between the cases with and without external field [Fig. 2(d)]. Darker regions show a higher electron concentration.

As mentioned before, we are interested in the effect of the incoming primary beam electrons in providing the necessary kick to cause emission. Therefore, in the next part we look into how the beam affects the orbitals.

In a typical experiment, the primary beam energy is 5 keV and its current about 0.5 pA. This means that the electrons are traveling at about 40 m/ μ s and arriving at the target at a rate of roughly 3 e/ μ s. So, there is roughly

one electron in every 13 m of the beam length (if we imagine a very long beam). In other words, electrons from the primary beam hit the nanotube tip one by one, quite independently of one another (no space charge effects). Since the electron beam scans an area around the nanotube, we considered three positions of the incoming electron with respect to the tube tip: outside the tube, but very close [Fig. 3(a)], inside the tube, at a small distance from the tip [Fig. 3(b)], and inside the tube at the center of the tip [Fig. 3(c)]. We have treated the beam electrons as point charges although a more rigorous model would have to consider the extent of the electron wave packet.

As seen before on Fig. 2(c), a 0.5 V/\AA field (typical of the experimental value) corresponds to the occupied energy levels being shifted up to very close to the emission barrier top (to within $\sim 0.4 \text{ eV}$ of the barrier top). Therefore, we used this value of field together with the different locations of the incoming electron. We calculated the energy levels of the system for all these cases (Fig. 4). When the beam reaches the vicinity of the tube just outside, it still induces no significant rise in the tube energy levels with respect to the emission barrier top: In the case of Fig. 4(a), the HOMO is still $\sim 0.4 \text{ eV}$ below the top of the emission barrier, similar to when there is no external electron beam [Fig. 2(c)]. If the incoming electron is inside the tube, a small distance away from the tip, there is a substantial upward shift in HOMO (about 1 eV) compared to the previous case, ending at $\sim 0.6 \text{ eV}$ above the barrier [Fig. 4(b)]. For comparison, DFT predicted HOMO at $\sim 0.8 \text{ eV}$ above the barrier in this case. In addition to raising some of the levels above the barrier top, this upward shift induces a substantial increase (exponential) in the tunneling current from the lower orbitals that now see a much thinner tunneling barrier in front of them. Once the scanning beam goes closer to the tube tip, the tube energy levels go down again with respect to the top of the emission barrier and emission stops [Fig. 4(c)]. This is because the rise in the local electronic potential energy due to the incoming electron is now having a strong effect on the vacuum level itself; since the potential due to an electron behaves as $1/r$, its effect on the vacuum level in the previous case where the incoming electron was a few angstroms away from the tip was very small. But this effect grows bigger as the electron approaches the tip and eventually becomes more important than the rise it creates in the nanotube energy levels. We can see on Fig. 4(c) that the emission barrier shape also shows the influence of the $1/r$ tail of the incoming electron's potential.

Even though the above rise in energy levels (about 1 eV) because of the primary electron was presented for the case where the nanotube was under external electric field, it is important to note that a similar situation happens with no external field, and the effect of the primary beam is rather independent of the external field. We redid the calculation in the presence of the incoming charge [as in Fig. 3(b)], but with no external field. In this case, the rise in HOMO was 1.13 eV . Therefore, in normal SEM imaging, a similar

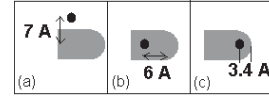


FIG. 3. Top view of the position of the incoming electron relative to the nanotube: (a) outside the tube on the side, (b) inside the tube about 6 \AA away from the tip, and (c) inside the tube at the center of the tip.

effect leads to enough secondary electron emission from the nanotube that makes it observable without difficulty.

In addition to the rise in energy levels, it is important to see how the nanotube electrons relocate themselves in response to the incoming electron. We plotted the difference in the nanotube charge distribution between the cases where there is an incoming electron in the nanotube $\sim 6 \text{ \AA}$ from the tip and where the incoming electron is at the center of the tip [Fig. 4(d)] (note: the incoming electron is from the external electron beam and is not to be confused with the nanotube electrons, the spatial distribution of which is being looked at here). Darker regions correspond to a more negative charge. Note that when the incoming electron is a little away from the tip, the nanotube electrons are pushed toward the tip. As we recall from Fig. 4(b), this is when there is strong emission. If the incoming electron is placed inside the tip itself, it tends to push the nanotube electrons away from the tip as evidenced by Fig. 4(d), and this is when emission stops. This corresponds to when the effect of the incoming electron in raising the emission barrier is higher than its effect in raising the orbital energies [see the energy levels in Fig. 4(c)].

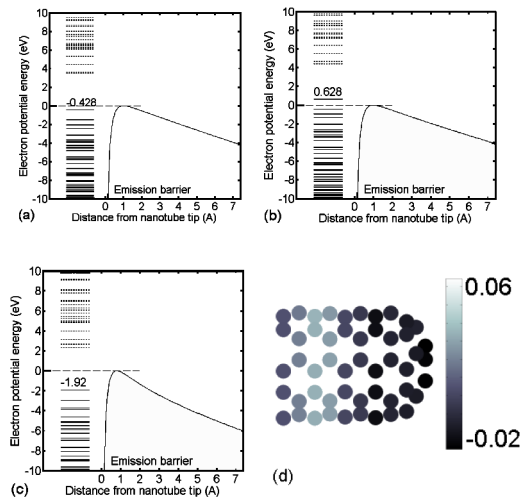


FIG. 4 (color online). Energy levels with an external field of $\sim 0.5 \text{ V/\AA}$ for different locations of the incoming electron: (a) outside the tube on the side, (b) inside the tube about 6 \AA away from the tip, and (c) inside the tube at the tube tip. (d) Difference in the nanotube charge distribution between the cases where there is an incoming electron in the nanotube $\sim 6 \text{ \AA}$ from the tip [as in Fig. 3(b)] and where the incoming electron is at the center of the tip. Darker regions correspond to more negative charge.

Note that so far we have assumed that the orbitals around or above the emission barrier will naturally emit. However, one has to consider the fact that as an electron from one of these orbitals starts to leave the nanotube, there will be a positive charge left behind, and the attraction from this positive charge might hinder the emission process. In the experiment, the nanotube is connected to a large reservoir of electrons. So, if the dielectric relaxation time of the nanotube is smaller than the time it takes for an electron to emit from the nanotube, electrons from the reservoir will replenish the lost negative charge and keep the nanotube neutral during the emission process. So, our arguments so far hold for the case where dielectric relaxation in the nanotube is faster than emission. If this is not the case, however, there will be a positive charge left behind. So, we redid the calculation of Fig. 4(b) (the emitting case), but this time also included one positive charge left on the nanotube surface (distributed uniformly). The result shows that emission still takes place in this case, but at a threshold of about 0.8 eV for the applied electric field. This means that the model can explain the electron emission process regardless of the relative values of nanotube dielectric relaxation time and emission time.

We note that the present study neglects the dynamic effects and the primary beam kinetic energy. Also, as mentioned previously, one has to take into account the wave nature of the electron for an exact treatment of the problem. Future work includes the extension of the model to include such effects. However, we have performed the experiments using a relatively wide range of primary beam energies (500 eV to 20 keV), and have observed the emission effect over the whole range. This independence of the effect from the primary beam kinetic energy further justifies the use of a static model such as the one presented here to explain the basic phenomenon.

The high electron multiplication factor (measured up to 100) in emission from the nanotube tip could have interesting implications for electron multipliers and detection devices. Also, in this process, a number of electrons might be emitted all at once or with some interesting correlation in their emission time. Therefore, the electron beam that is produced might have interesting properties (e.g., reduced shot noise) that are absent in the current electron sources or in the secondary electrons emitted from bulk samples under normal SEM conditions.

Summary.—Traditional electron beam–bulk specimen interaction models are not capable of explaining the high secondary electron emission from a nanotube being imaged in a scanning electron microscope. We presented a new model for the beam–nanotube interaction and generation of secondary electrons. We used *ab initio* calculations to show that an extra electron placed inside the nanotube can raise the energy levels by about 1 eV, thus assisting them in overcoming the work function barrier. This explains why nanotubes, despite their extremely small diameters, can easily be seen in an electron microscope. Also,

we saw that if the nanotube is already biased near the field-emission threshold, this rise in energy levels is enough to trigger a full-scale emission from the tip. Although used here to explain how nanotube images are formed in an electron microscope, the approach may be used in modeling the interaction of charged particles (electrons or ions) with various nanostructures for other applications such as electron detection and amplification.

We thank Professor Hongjie Dai for providing nanotube growth facilities and the Stanford Bio-X and the San Diego supercomputer centers for computational resources. B. S. acknowledges support from an NSF grant on Network for Computational Nanotechnology (NCN). This work was partially supported by the U.S. Department of the Air Force under Contract No. F33615-00-1-1728, the DARPA ALP, and NSF NIRT (ECS 0210899). Fabrication was performed in part at the Stanford Nanofabrication Facility of NNIN supported by the National Science Foundation under Grant No. ECS-9731293.

*Author to whom correspondence should be addressed.

Electronic address: anojeh@stanford.edu

- [1] Sh. Fan, M. G. Chapline, N. R. Franklin, T. W. Tombler, A. M. Cassell, and H. Dai, *Science* **283**, 512 (1999).
- [2] O.-J. Lee and K.-H. Lee, *Appl. Phys. Lett.* **82**, 3770 (2003).
- [3] K. A. Dean and B. R. Chalamala, *Appl. Phys. Lett.* **76**, 375 (2000).
- [4] A. Nojeh, W.-K. Wong, A. W. Baum, R. F. Pease, and H. Dai, *Appl. Phys. Lett.* **85**, 112 (2004).
- [5] A. Nojeh, W.-K. Wong, E. Yieh, R. F. Pease, and H. Dai, *J. Vac. Sci. Technol. B* **22**, 3124 (2004).
- [6] L. Luo, L.-M. Peng, Z. Q. Xue, and J. L. Wu, *Phys. Rev. B* **66**, 155407 (2002).
- [7] G. Zhou and Y. Kawazoe, *Phys. Rev. B* **65**, 155422 (2002).
- [8] Ch. Kim, B. Kim, S. M. Lee, Ch. Jo, and Y. H. Lee, *Phys. Rev. B* **65**, 165418 (2002).
- [9] G. Zhou, W. Duan, and B. Gu, *Phys. Rev. Lett.* **87**, 095504 (2001).
- [10] D. C. Joy, *Monte Carlo Modeling for Electron Microscopy and Microanalysis* (Oxford University Press, New York, 1995).
- [11] S. Han, Ph.D. dissertation, Seoul National University, 2000.
- [12] S. Han, M. H. Lee, and J. Ihm, *Phys. Rev. B* **65**, 085405 (2002).
- [13] X. Zheng, G.-H. Chen, Zh. Li, Sh. Deng, and N. Xu, *Phys. Rev. Lett.* **92**, 106803 (2004).
- [14] R. Saito, G. Dresselhaus, and M. S. Dresselhaus, *Physical Properties of Carbon Nanotubes* (Imperial College Press, London, 1999).
- [15] M. J. Frisch *et al.*, GAUSSIAN 98, Revision A.7, Gaussian, Inc., Pittsburgh, PA, 1998.
- [16] A. S. Barnard, S. P. Russo, and I. K. Snook, *Philos. Mag. B* **82**, 1767 (2002).
- [17] A. Rosen, D. E. Ellis, H. Adachi, and F. W. Averill, *J. Chem. Phys.* **65**, 3629 (1976).